Arabian Journal of Chemistry (2022) **15**, 103771

King Saud University

Arabian Journal of Chemistry

www.ksu.edu.sa
www.sciencedirect.com

ORIGINAL ARTICLE

Synthesis, self-assembly and optical properties of novel fluorescent alkoxy-substituted fluoroaryl 1, 3, 4-oxadiazole organogelator

Aisha Hossan [a], Hana M. Abumelha [b], Rua B. Alnoman [c], Abrar Bayazeed [d], Amerah Alsoliemy [d], Ali A. Keshk [e], Nashwa M. El-Metwaly [d,f,*]

[a] *Chemistry Department, Faculty of Science, King Khalid University, Abha, Saudi Arabiaf*
[b] *Department of Chemistry ,College of Science, Princess Nourah bint Abdulrahman University, P.O. Box 84428, Riyadh 11671, Saudi Arabia*
[c] *Department of Chemistry, College of Science, Taibah University, Madinah, P.O. Box 344, Saudi Arabia*
[d] *Department of Chemistry, Faculty of Applied Science, Umm-Al-Qura University, Makkah 24230, Saudi Arabia*
[e] *Depertment of Chemistry, Faculty of Science, Tabuk University, Tabuk-71491, Saudi Arabia*
[f] *Department of Chemistry, Faculty of Science, Mansoura University, El-Gomhoria Street 35516, Egypt*

Received 23 September 2021; accepted 3 February 2022
Available online 7 February 2022

KEYWORDS

Aromatic nucleophilic substitution;
Decarboxylation cross-coupling;
1, 3, 4-Oxadiazole;
Fluorescence;
Organogelator

Abstract Aromatic nucleophilic substitution (S_NAr) reactions have been known to be regioselective to the para position on a variety of substituted perfluorobenzenes. In the current study, a series of fluoroaryl 1, 3, 4-oxadiazole derivatives substituted with different para terminal ethers were synthesized using S_NAr chemistry to afford fluorescent and thermally reversible low molecular weight organogelators (LMWOs). S_NAr was used to synthesize these highly fluorinated organogelators in high purity and good yields starting from pentafluorobenzoic acid and 4′-hydroxy-4-biphenylcarbonitrile. These fluorinated 1, 3, 4-oxadiazole derivatives were characterized by elemental analysis, FTIR, and ^{1}H, ^{13}C, and ^{19}F NMR spectroscopy. The photophysical properties of those organogelators were described. Both UV–visible absorption and fluorescence spectral profiles displayed a solvatochromic and solvatofluorochromic properties. The absorption maxima for the developed organogelators were monitored in the range of 260–289 nm, whereas the emission maxima were monitored in the range of 278–305 nm. The best gelation properties were monitored for the hexyloxy-substituted 2-(biphenylyl)-5-(perflurophenyl)-1, 3, 4-oxadiazole gelator in different solvents with critical gel concentrations in the range of 1.86–5.07 mM. The self-assembly process

* Corresponding author.
E-mail addresses: ahossan@kku.edu.sa (A. Hossan), Rua-b-n@live.co.uk (R.B. Alnoman), aabayazeed@uqu.edu.sa (A. Bayazeed), amsolieme@uqu.edu.sa (A. Alsoliemy), akeshk@ut.edu.sa (A.A. Keshk), nmmohamed@uqu.edu.sa (N.M. El-Metwaly).
Peer review under responsibility of King Saud University.

Production and hosting by Elsevier

https://doi.org/10.1016/j.arabjc.2022.103771

was monitored to occur via van der Waals forces and π-π stacks to result in gelation of solvents. Scanning electron microscope (SEM) demonstrated nanofiber-like structures (350–550 nm). The thermal stability of the hexyloxy-substituted organogel was monitored at 48 °C. Both cytotoxicity and antimicrobial activity of the produced fluoroaryl 1, 3, 4-oxadiazole derivatives were explored to verify their potential use for biomedical applications, such as drug delivery and bioimaging.

1. Introduction

LMWOs have been attractive materials owing to their thermal reversibility, diversity of their micro(nano) scaffolds and chemical sensitivity (Aykent et al., 2019; Peveler et al., 2018; Sasaki et al., 2018). Gelators were typically used in a variety of applications, like cosmetics, foodstuff and pharmaceutical purposes. They have been able to generate non-covalent self-assembled physical texture of unique features (Kim et al., 2020; Zhang et al., 2019). Fluorine-containing substances have received substantial interest in numerous fields, such as polymers, pesticides, pharmaceuticals and liquid crystals. Moreover, the perfluorinated compounds typically establish a rough surface with the ability to introduce superhydrophobic and self-cleanable surfaces (Fan et al., 2019; Guerre et al., 2018; Zhang et al., 2018). The presence of fluorine atoms in molecular structures can stimulate liquid crystalline performance better than their non-fluorinated counterparts, which can be ascribed to the bigger size of fluorine in comparison to hydrogen to result in substantial steric effects. Fluorine-substituted liquid crystals usually exhibit a variety of nematic mesogenic phases (Yamada et al., 2017; Zhang et al., 2017). Perfluoroaromatics are highly reactive for cross-couple reactions. The synthesis of perfluoroaryls from the corresponding aromatic tetrazoles and pentafluorobenzoic acid has been recently achieved. This synthetic approach employed cheap and less sensitive compounds. Therefore, this synthetic strategy can substitute the costly and highly sensitive organometallic compounds, like $PdCl_2$ (Feng et al., 2012). An extensive research has been reported on the application of transition metals as catalytic agents in the common synthetic methods of fluorine-containing compounds. Nonetheless, those approaches suffer some difficulties, including low yield and poor selectivity. Furthermore, extensive amounts of by-products are usually monitored due side reactions causing extra purification cost (Altoom et al., 2021).

S_NAr has been an essential synthetic procedure, in which a nucleophile compound replaces a high-quality leaving group on an aryl moiety. S_NAr of fluorine-containing aromatic compounds by a diversity of nucleophilic compounds has been explored for aromatic moieties with strong electron withdrawing groups, like nitro, sulphonyl, cyano and polyhalogen to result in high yield and fast reaction rate (Bidusenko et al., 2020; Tominaga et al., 2020). S_NAr typically occurs in an aprotic solvent, such as dimethylacetamide, hexamethylphosphoramide, dimethyl sulfoxide and dimethylformamide in the temperature range of 25–100 °C, which typically relies on the activation energy required by the aromatic moiety. For instance, spiropyrrolidone-3, 3′-oxoindole has been the key skeleton for many natural materials with optical activity. Organocatalyzed (enantio-)regio-selective S_NAr chemistry was efficiently carried out between 1, 3-dicarbonyls and reactive aromatic moiety (Hicks et al., 2020). The phase transfer catalysis has been applied to provide the optically active spiropyrrolidone-3,3′-oxoindoles in good yield under mild conditions. Unexpectedly, no studies have been reported on the development of LMWO based on fluorine-containing 1, 3, 4-oxadiazoles despite their significant role in a variety of recent optoelectronic advances. Oxadiazoles are heterocyclic substances comprising five membered ring with two nitrogen atoms and one oxygen atom (Marti et al., 2003; Vaidya et al., 2021). They have been used for a variety of valuable biological purposes and drug systems, such as antiviral raltegravir, analgesic, anti-depressive, antimicrobial furamizole, anti-diabetic, anti-inflammatory and anticancer zibotentan (Glomb et al., 2021; Patel et al., 2014; Salahuddin et al., 2017; Verma et al., 2019).

Herein, we describe the first fluorescent organogelator with a rigid perfluoroaryl 1, 3, 4-oxadiazole core and flexible terminal alkyl tails. The preparation and photophysical performance were studied. The reaction between penetafluorobenzoic and the appropriate tetrazole-substituted aryl introduced an extended conjugation of rigid 1, 3, 4-oxadiazole core with a strong fluorescence, solvatochromism and solvatofluorochromism properties. A suitable synthesis of perfluoroaryl 1, 3, 4-oxadiazole bearing ethers were carried out via S_NAr. The chemical structures of the prepared alkoxy-substituted perfluoroaryl 1, 3, 4-oxadiazoles were investigated by $^1H/^{13}C/^{19}F$ NMR, elemental analysis and FT-IR spectra. The prepared oxadiazole derivatives exhibited fluorescence in the ultraviolet spectrum range (10–400 nm); thus, they can be reported as appropriate materials with lower energy consumption, such as handy and flexible electronic displays (Lin et al., 2017; Ragni et al., 2018). The gelation properties and supramolecular assembly of the current oxadiazole derivatives were inspected in some organic solvents. Such assembly could be attributed to physical bond formation leading to formation of intertwined fibrillar textures able to immobilize solvents. Both cytotoxic and antimicrobial behaviors of the prepared oxadiazole derivatives were explored. SEM analysis showed novel fluorescent nanofibrous entanglements self-assembled from the organogelators. Thus, the current oxadiazole organogelators can be considered as appropriate candidates for a variety of biomedical applications, such as bioimaging and drug delivery systems.

2. Experimental

2.1. Materials

Chemicals were supplied from Merck and Frontier-Scientific (Egypt). Solvents (spectroscopic grade) were purchased from Merck and Fluka. Silia Flash F60 silica gel was employed for

column chromatography. TLC plates of silica gel were employed for naked-eye monitoring of reaction progress. The intermediates **1**–**3** were prepared according to preceding procedures (Jedlovská et al., 1994; Radwan et al., 2021; Tandon et al., 2001) from commercial compounds; 4-Hydroxy-4′-cyanobiphenyl and pentafluorobenzoic acid (Merck; Egypt).

2.2. Methods

Melting points were measured by differential scanning calorimetry (TA2920). NMR spectra were studied by BRUKER AVANCE 400 MHz. Infrared spectra were studied by JASCO-4700. The elemental analysis was evaluated by Norwalk Perkin-Elmer 2400 (United States). UV–visible absorption spectral curves were evaluated by HP-8453. VARIAN CARY ECLIPSE was employed to evaluate both fluorescence spectral curves (sol and gel), and quantum yield (Φ). In order to report the emission spectra of gel, the generated gel was stirred on a shaker for 5 min. Ethanolic solutions of rhodamines, including 6G (Φ_r = 0.95) and 101 (Φ_r = 0.96) were utilized as standards to determine the quantum yields. SEM images were taken by Quanta FEG250 (Czech) as the organogel in *n*-propanol was subjected to casting on a glass substrate and left to dry under ambient conditions to give xerogel that was annealed overnight at 45 °C, and covered with a thin layer of gold (∼10 nm).

2.3. Gel formation

The gel formation tests were carried out by dissolving the prepared oxadiazole derivatives **4a-c** in different solvents by exposure to heat toward the boiling point followed by cooling. The solutions were then left to settle down as the organogel was generated in 25–45 min relying on the gelator total content. The reversibility between sol-to-gel and gel-to-sol was investigated by keeping the vial containing the gel reverted in an oil bath. The vial was subjected to heating, and the temperature at which the gel was observed to collapse was recorded as the gel melt temperature. This procedure was repeated some cycles to verify excellent reversibility.

2.4. Cytotoxic assay

The cytotoxic assay of the alkoxy-substituted 2-(biphenylyl)-5-(perflurophenyl)-1, 3, 4-oxadiazole derivatives was evaluated *in vitro* utilizing immortalized normal skin fibroblasting cells (BJ1) using previous proliferating MTT method (Plastina et al., 2012).

2.5. Antimicrobial properties

The antimicrobial performance of the alkoxy-substituted 2-(bi phenylyl)-5-(perflurophenyl)-1, 3, 4-oxadiazole derivatives was examined under standard procedures against ***S. aureus*** (ATCC 25923), and ***E. coli*** (ATCC 25922) (Ghasemi et al., 2018).

2.6. Synthetic approaches

2.6.1. Synthesis of 4′-hyxyloxy-4-biphenylcarbonitrile (1)

An admixture of 4′-hydroxy-4-biphenylcarbonitrile (10 mmol), potassium carbonate (20 mmol), and a bit of potassium iodide was added to dimethylformamide (20 mL). Then, 1-iodohexane (10 mmol) was added and the admixture was exposed to heat over 12hrs at 70 °C. The cold admixture was decanted into water; the precipitate was filtered and rinsed with hexane. White powder was obtained (74%); ^{1}H NMR (400 MHz, $CDCl_3$): 7.98 (d, 4H; aromatic CH), 7.83 (d, 2H; aromatic CH), 7.05 (d, 2H; aromatic CH), 4.08 (t, 2H; aliphatic CH), 1.81 (q, 2H; aliphatic CH), 1.44–1.52 (m, 2H; aliphatic CH), 1.29–1.33 (m, 2H; aliphatic CH), 1.27 (t, 2H; aliphatic CH), 0.91 (t, 3H; aliphatic CH).

2.6.2. Synthesis of 4-hexyloxy-4′-(tetrazolyl)biphenyl (2)

A mixture of 4-hexyloxy-4′-cyanobiphenyl (10 mmol), NaN_3 (20 mmol), and lithium chloride (0.03 mol) was added to *N*-methyl-2-pyrrolidone (15 mL). The admixture was stirred at 130 °C for 3 days, cooled and decanted into water, acidified to pH 2–3, filtered and rinsed with excess of hexane. The resultant material was recrystallized from propyl alcohol to provide a white residue (86%); ^{1}H NMR (400 MHz, $CDCl_3$): 10.45 (s, 1H; tetrazole NH), 8.25 (d, 2H; aromatic CH), 8.02 (d, 2H; aromatic CH), 7.88 (d, 2H; aromatic CH), 6.98 (d, 2H; aromatic CH), 4.05 (t, 2H; aliphatic CH), 1.82 (q, 2H; aliphatic CH), 1.40–1.47 (m, 2H; aliphatic CH), 1.30–1.34 (m, 2H; aliphatic CH), 1.21 (t, 2H; aliphatic CH), 0.93 (t, 3H; aliphatic CH).

2.6.3. Synthesis of 2-[4′-(hexyloxy)[1,1′-biphenyl]-4-yl]-5-[2,3,4,5,6-pentaflurophenyl]-1, 3, 4-oxadiazole (3)

A mixture of 4-hexyloxy-4′-(tetrazolyl)biphenyl (10 mmol), pentafluorobenzoic acid (10 mmol), and *N*, *N*′-dicyclohexylcar bodiimide (0.05 mol) was added to *N*-methyl-2-pyrrolidone (15 mL). The admixture was stirred at 130 °C for 3hrs, cooled and decanted into water, acidified to pH 2–3, filtered and rinsed with excess of hexane. The product was re-crystallized from a mixture of ethanol and chloroform (1:1) to give a white residue (72%); ^{1}H NMR (400 MHz, $CDCl_3$): 8.20 (d, 2H; aromatic CH), 7.76 (d, 2H; aromatic CH), 7.62 (d, 2H; aromatic CH), 7.02 (d, 2H; aromatic CH), 4.05 (t, 2H; aliphatic CH), 1.81–1.87 (m, 2H; aliphatic CH), 1.57–1.62 (m, 2H; aliphatic CH), 1.39 (m, 4H; aliphatic CH), 0.96 (t, 3H; aliphatic CH); IR (neat, ν/cm^{-1}): 3071 (aryl stretch vibrations of CH), 2921 and 2853 (aliphatic asymmetric stretch vibrations of CH), 1555 (C═N), 1488 (aryl bend vibrations of C═C), 1382 (C-O), 1206 (bend vibrations of CH_2), 1069 (bend vibrations of CH_3), 840 (aryl bend vibrations of CH), 761 (bend rock vibrations of CH_2).

2.6.4. General procedure for the preparation of 2-[4′-(hexyloxy)[1,1′-biphenyl]-4-yl]-5-[2,3,5,6-tetrafluro-(4-alkyloxy)phenyl]-1, 3, 4-oxadiazole (4)

An admixture of 2-[4′-(hexyloxy)[1,1′-biphenyl]-4-yl]-5-[2,3,4,5,6-pentafluorophenyl]-1, 3, 4-oxadiazole (1 mmol) and anhydrous DMF was heated till complete dissolution. The corresponding alcohol (1 mmol) was added. After cooling, *t*-BuOK was added to the admixture. Upon reaction completion, the mixture was subjected to rotary evaporator, and the solid residue was re-crystallized.

2.6.5. Synthesis of 2-[4′-(hexyloxy)[1,1′-biphenyl]-4-yl]-5-[2,3,5,6-tetrafluro-(4-ethoxy)phenyl]-1, 3, 4-oxadiazole (4a)

Prepared from 2-[4′-(hexyloxy)[1,1′-biphenyl]-4-yl]-5-[2,3,4,5,6-pentafluorophenyl]-1, 3, 4-oxadiazole (215 mg, 0.45 mmol), dimethylformamide (10 mL), excessive amount of ethanol (5 mL), and *t*-BuOK (65 mg). The solid residue was subjected to re-crystallization from propyl alcohol to provide a white residue (53%); mp 125–127 °C; ^{1}H NMR (400 MHz, $CDCl_3$): 8.15 (d, 2H; aromatic CH), 7.74 (d, 2H; aromatic CH), 7.60 (d, 2H; aromatic CH), 7.01 (d, 2H; aromatic CH), 4.49 (q, 2H; aliphatic CH), 4.03 (t, 3H; aliphatic CH), 1.80–1.86 (m, 2H; aliphatic CH), 1.49–1.53 (m, 2H; aliphatic CH), 1.34–1.38 (m, 6H; aliphatic CH), 0.94 (t, 3H; aliphatic CH); ^{13}C NMR (400 MHz, $CDCl_3$): 165.39, 159.56, 155.52, 146.69, 144.63, 143.98, 142.52, 139.91, 131.81, 128.83, 128.22, 127.64, 127.16, 121.22, 115.01, 78.18, 68.17, 31.60, 29.22, 25.73, 22.62, 15.50, 14.05; ^{19}F NMR ($CDCl_3$): −146 (q, 2F), −157 (q,2F); IR (neat, ν/cm^{-1}): 3078 (aryl stretch vibrations of CH), 2924 and 2865 (aliphatic asymmetric stretch vibrations of CH), 1596 (C = N), 1512 (aryl bend vibrations of C = C), 1337 (C-O), 1190 (bend vibrations of CH_2), 1121 (bend vibrations of CH_3), 864 (aryl bend vibrations of CH), 723 (bend rock vibrations of CH_2); Elemental analysis (514.19; $C_{28}H_{26}F_4N_2O_3$): calculated: C 65.36, H 5.09, N 5.44; Detected: C 65.27, H 5.18, N 5.32.

2.6.6. Synthesis of 2-[4′-(hexyloxy)[1,1′-biphenyl]-4-yl]-5-[2,3,5,6-tetrafluro-(4-hexyloxy)phenyl]-1, 3, 4-oxadiazole (4b)

Prepared from 2-[4′-(hexyloxy)[1,1′-biphenyl]-4-yl]-5-[2,3,4,5,6-pentaflurophenyl]-1, 3, 4-oxadiazole (120 mg, 0.25 mmol), dimethylformamide (5 mL), hexanol (2 mL; excess), and *t*-BuOK (35 mg). The solid residue was subjected to re-crystallization from propyl alcohol to provide a white residue (48%); mp 121–123 °C; ^{1}H NMR (400 MHz, $CDCl_3$): 8.18 (d, 2H; aromatic CH), 7.71 (d, 2H; aromatic CH), 7.66 (d, 2H; aromatic CH), 7.01 (d, 2H; aromatic CH), 4.51 (q, 2H; aliphatic CH), 4.05 (q, 2H; aliphatic CH), 1.79–1.84 (m, 2H; aliphatic CH), 1.52–1.56 (m, 2H; aliphatic CH), 1.33–1.39 (m, 12H; aliphatic CH), 0.92 (t, 6H; aliphatic CH); ^{13}C NMR (400 MHz, $CDCl_3$): 164.88, 158.47, 154.55, 147.70, 145.03, 142.99, 141.63, 138.84, 130.99, 129.75, 128.31, 127.55, 126.06, 120.04, 115.00, 77.27, 69.20, 30.48, 28.47, 25.65, 24.83, 22.00, 21.71, 16.31, 15.28, 14.26; ^{19}F NMR ($CDCl_3$): −146 (q, 2 F), −157 (q, 2 F); IR (neat, ν/cm^{-1}): 3071 (aryl stretch vibrations of CH), 2925 and 2869 (aliphatic asymmetric stretch vibrations of CH), 1590 (C = N), 1511 (aryl bend vibrations of C = C), 1344 (C-O), 1185 (bend vibrations of CH_2), 1117 (bend vibrations of CH_3), 858 (aryl bend vibrations of CH), 731 (bend rock vibrations of CH_2); Elemental analysis (570.25; $C_{32}H_{34}F_4N_2O_3$): calculated: C 67.36, H 6.01, N 4.91; Detected: C 67.21, H 5.92, N 5.03.

2.6.7. Synthesis of 2-[4′-(hexyloxy)[1,1′-biphenyl]-4-yl]-5-[2,3,5,6-tetrafluro-(4-decyloxy)phenyl]-1, 3, 4-oxadiazole (4c)

Prepared from 2-[4′-(hexyloxy)[1,1′-biphenyl]-4-yl]-5-[2,3,4,5,6-pentaflurophenyl]-1, 3, 4-oxadiazole (120 mg, 0.25 mmol), dimethylformamide (5 mL), decanol (2 mL; excess), and *t*-BuOK (35 mg). The solid residue was subjected to re-crystallization from propyl alcohol to provide a white powder (43%); mp 115–117 °C; ^{1}H NMR (400 MHz, $CDCl_3$): 8.21 (d, 2H; aromatic CH), 7.68 (d, 2H; aromatic CH), 7.61 (d, 2H; aromatic CH), 7.00 (d, 2H; aromatic CH), 4.48 (q, 2H; aliphatic CH), 4.07 (q, 2H; aliphatic CH), 1.81–1.87 (m, 2H; aliphatic CH), 1.51–1.57 (m, 2H; aliphatic CH), 1.35–1.41 (m, 24H; aliphatic CH), 0.92 (t, 3H; aliphatic CH), 0.89 (t, 3H; aliphatic CH); ^{13}C NMR (400 MHz, $CDCl_3$): 164.27, 157.00, 154.37, 148.08, 146.00, 142.65, 140.73, 138.58, 131.72, 129.13, 128.25, 127.51, 126.55, 121.38, 116.18, 78.22, 68.47, 30.51, 28.33, 28.00, 25.34, 24.92, 24.46, 22.35, 21.00, 20.89, 18.47, 18.05, 16.00, 15.39, 14.02; ^{19}F NMR ($CDCl_3$): −146 (q, 2F), −157 (q, 2F); IR (neat, ν/cm^{-1}): 3069 (aryl stretch vibrations of CH), 2927 and 2875 (aliphatic asymmetric stretch vibrations of CH), 1586 (C = N), 1507 (aryl bend vibrations of C = C), 1332 (C-O), 1178 (bend vibrations of CH_2), 1122 (bend vibrations of CH_3), 863 (aryl bend vibrations of CH), 725 (bend rock vibrations of CH_2); Elemental analysis (654.34; $C_{38}H_{46}F_4N_2O_3$): calculated: C 69.70, H 7.08, N 4.28; Detected: C 69.81, H 6.89, N 4.39.

3. Results and discussion

3.1. Chemistry and analysis

Both 4-hydroxy-4′-cyanobiphenyl and pentafluorobenzoic acid are commercially available. 4′-Hydroxy-4-biphenylcarbonitrile dissolved in DMF was subjected to treatment with 1-iodohexane and K_2CO_3 under ambient circumstances to give 4-alkoxy-4′-cyanobiphenyl in high yield as illustrated in Scheme 1 (Fouad et al., 2018; Jedlovská et al., 1994; Radwan et al., 2021; Tandon et al., 2001). The alkoxy-substituted 2-(biphenylyl)-5-(perflurophenyl)-1, 3, 4-oxadiazole derivatives were prepared in high yields from pentafluorobenzoic acid and aryl cyanide. The 2-biphenyl-substituted 1, 3, 4-oxadiazole can be prepared by adding the oxadiazole ring into the biphenyl moiety with the fitting terminal functional group. The molecular structures of the prepared alkoxy-substituted 2-(biphenylyl)-5-(perflurophenyl)-1, 3, 4-oxadiazoles were proved with elemental, FT-IR, ^{1}H/^{13}C/^{19}F NMR spectral analyses.

S_NAr reaction of an aryl moiety activated with perfluorination and alcoholates were assessed under non-forcing conditions. Those perfluorinated aromatic materials are stable and commercially available. Additionally, they have shown excellent reactivity toward S_NAr reaction under mild conditions (Altoom et al., 2021). In the current research study, alkoxy tails were inserted into the terminal positions of the aromatic moieties to allow a better self-assembly process via van der Waals forces (Table 1). S_NAr reactions have been reported as *para* specific on a variety of perfluoroaryls.

The produced 2-(biphenylyl)-5-(perflurophenyl)-1, 3, 4-oxadiazole derivatives were treated under S_NAr with different alcohols using DMF as a solvent and *t*-BuOK as a base. The reactivity of fluorine located at the *para* carbon atom of the benzene ring as a good leaving group in S_NAr arises from the existence of several fluorine substituents at both *ortho* and *meta* carbon atoms of benzene moiety. Therefore, a regio-selective S_NAr could be accomplished only at the *para* carbon atom by replacing the active *para* fluorine to provide perfluoroaryls bearing *para*-substituted alkyl ether group.

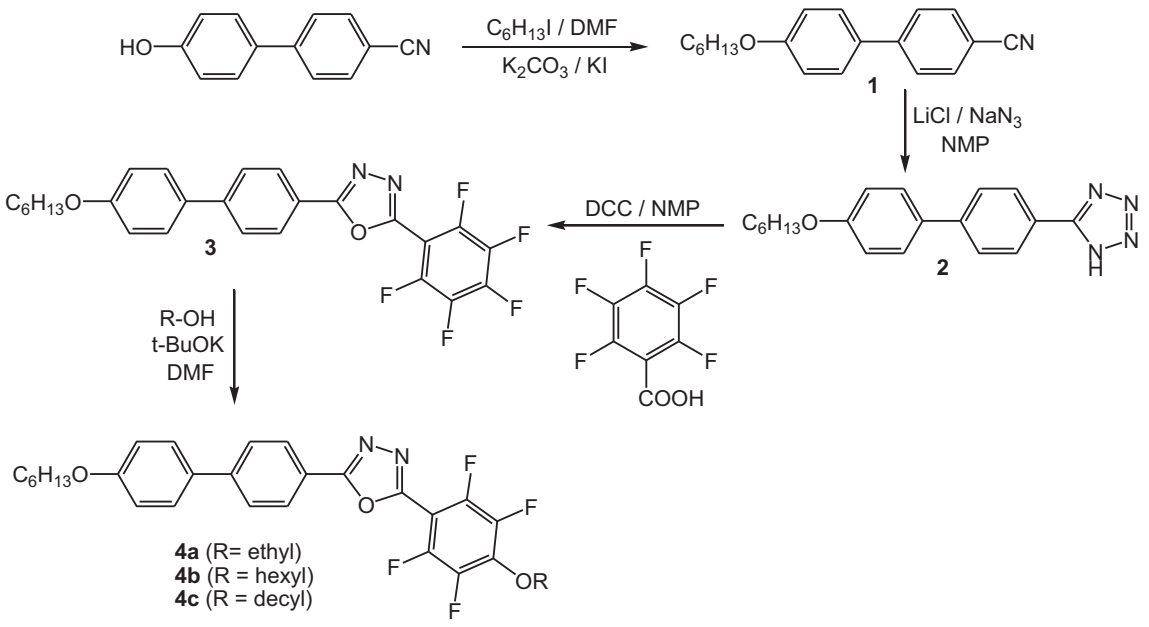

Scheme 1 Synthesis of alkoxy-substituted 2-(biphenylyl)-5-(perflurophenyl)-1, 3, 4-oxadiazole derivatives.

3.2. Photophysical measurements

Stimuli-responsive materials can be applied to introduce smart materials and products able to switch their absorbance and/or emissive properties in responding to external stimuli, like solvent polarity and temperature (Khattab et al., 2020). Thus, both UV–visible absorption and emission spectral properties of the prepared oxadiazole derivatives were inspected in some selected solvents (Fig. 1). The maximum absorption wavelength was reported to display strong Stoke's shift as summarized in Table 2. The photophysical spectra (UV–Vis absorption and emission spcetra) were measured in various solvents, including tetrahydrofuran, hexane, dichloromethane, dimethyl sulfoxide and ethanol in diluted solutions to assure a complete dissolution. All oxadiazole derivatives absorb in the ultraviolet range. These absorbance bands can be attributed to π-π* transition. The absorption wavelength of the oxadiazole derivatives with lower length of alkoxy tails displayed slightly lower values compared to oxadiazoles with higher length of alkoxy tails. Thus, a bathochromic shift was monitored with extending the alkyl tail length. All oxadiazoles emit in the near ultraviolet-blue range. Nonetheless, a minor hypsochromic shifting was monitored in the fluorescent spectra with extending the alkyl tail length. This could be attributed to the energy of the excited state which decreases with extending the alkyl tail length leading to high emission character.

Table 1 Alkoxy-substituted 2-(biphenylyl)-5-(perflurophenyl)-1, 3, 4-oxadiazole derivatives and the yields produced from S_NAr.

Gelator	R	R'	Yield (%)
4a	Hexyl	Ethyl	53
4b	Hexyl	Hexyl	48
4c	Hexyl	Decyl	43

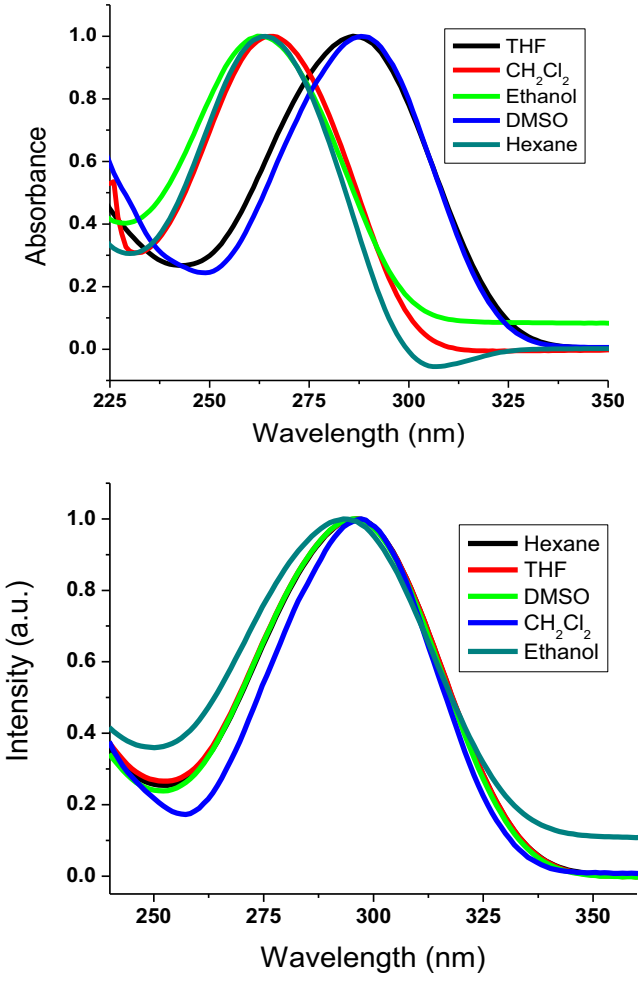

Fig. 1 Normalized UV–visible absorbance (a) and fluorescence (b) spectral analysis of **4b** under ambient conditions.

Table 2 UV–visible absorbance (A) and fluorescence (F) wavelengths in different solvents.

Solvent		4a	4b	4c
Hexane	A	262	264	268
	F	286	295	304
DMSO	A	284	287	289
	F	289	295	299
EtOH	A	260	262	266
	F	278	293	301
THF	A	280	285	288
	F	296	295	300
CH_2Cl_2	A	263	265	272
	F	285	297	305

Thus, the oxadiazole derivatives with lower length of alkoxy tails exhibit good charge transfer/conformational repose in the excited form. The lower radiation of oxadiazole derivatives with higher length of alkoxy tails can be ascribed to the strong twist ability of the peripheral fluorine-containing phenyl ring owing to the fluoro-atoms at the bay locations amid the fluorine-containing benzene and oxadiazole moieties. On the other hand, the oxadiazole derivatives with lower length of alkoxy tails displayed a higher radiation/emission property owing to expanded planar conjugate molecular system of oxadiazole core and peripheral aryl moieties. Additionally, fluorine substitution should considerably improve the intramolecular charge transfer (ICT) compared to nonfluorinated derivatives (Radwan et al., 2021).

The current alkoxy-substituted 2-(biphenylyl)-5-(perfluro phenyl)-1,3,4-oxadiazole derivatives composed of electron-donating terminal alkoxy tails bonded to a conjugate core of electron-accepting fluorine-containing aromatic moiety. Such molecular systems with push–pull ICT character are susceptible to solvatochromism and solvatofluorochromism properties monitored in various solvents of different polarity. Both UV–visible absorbance and fluorescence spectral profiles showed an increment in the maximum wavelength with the increase of the solvents polarities demonstrating positive solvatochromic and solvatofluorochromic properties. This bathochromic shifting reflects that the excited form is more polar than the ground form as the perfluorinated molecular systems are more stable in polar solvents. Inserting fluorine substituents can stimulate extraordinary features in comparison to the nonfluorinated counterparts. This could be ascribed to the large diameter of fluoro-atom compared to hydrogen causing substantial steric effects leading to higher quantum yield [12]. Hence, the oxadiazole derivatives, including **4a**, **4b** and **4c** demonstrated better quantum yields in comparison to those of the nonfluorinated oxadiazole counterparts (Gong et al., 2019). However, the quantum yield values were monitored to decrease with the increase of the alkyl tail length.

3.3. Organogel study

Nanofibrous entanglements were formed by self-assembled of alkoxy-substituted π-conjugated 2-(biphenylyl)-5-(perflurophe nyl)-1, 3, 4-oxadiazole derivatives. Fluorescence has been a critical property with the ability to show a responsive emission change to an external stimulus. Fluorescent architectures display remarkable reversible changes in both intensity and color due to self-assembly. Therefore, fluorescence architectures have been reported as useful sensors for the detection of various analytes (Ma et al., 2018). No organogel was formed for the prepared perfluorinated intermediate; 2-[4′-(hexyloxy)[1,1′ -biphenyl]-4-yl]-5-[2,3,4,5,6-pentaflurophenyl]-1, 3, 4-oxadiazole **3**. The synthesized alkoxy-substituted 2-(bipheny lyl)-5-(perflurophenyl)-1,3,4-oxadiazole organogelators consisted of two ether tails isolated by 2-(biphenylyl)-5-(perfluro phenyl)-1, 3, 4-oxadiazole core. The rigid aromatic core was accountable for π-π stack, whereas the terminal alkyl chains were accountable for van der Waals forces. Concerning the self-assembly process of those fluorinated organogelators, the molecular aggregation provides three dimensional nanofibrous entanglements, which can be subjected to control by the opposed parameters occuring from their dissolution and crystal creation. The oxadiazole derivatives, including **4a, 4b** and **4c** can be dissolved in a number of solvents only upon heating to elevated temperatures. Upon dissolving organogelator under gentle heating, and then cooling back, a solid-like oganogel was generated as demonstrated in Fig. 2. The formation of organogels was studied in different solvents. The values of the critical gel concentrations for **4b** were monitored at 1.86–5.07 mM. The organogelator **4b** demonstrated a considerable gelation of solvents, such as *n*-butanol (1.86 mM), *n*-octanol (2.61 mM), toluene (3.14 mM) and 1, 2-dichloroethane (5.07 mM). However, compound **4b** demonstrated partial gelation in tetrahydrofuran, acetonitrile and dimethylsulfoxide. Additionally, it displayed no gelation in dichloromethane, *n*-propanol, ethylacetate and chloroform due to its high solubility. The gelation properties of the different oxadiazole derivatives are displayed in Table 3. The generated organogels exhibited colorless appearance. The sol-to-gel switch course is thermally reversible. All organogels exhibited photophysical properties comparable to those in dilute solutions. Additionally, the gels produced from **4b** in *n*-butanol and *n*-octanol displayed high stability for a few weeks, whereas the gels produced from **4b** in toluene and 1, 2-dichloroethane were stable only for a few days.

Increasing the alkyl chain length improved the formation ability of organogel. However, the hexloxy-substituted oxadiazole **4b** demonstrated a better gel formation in comparison to the decyloxy-substituted oxadiazole **4c**. This can be ascribed to the high dissolution ability of **4c** in organic solvent directed by the long decyloxy chain. The type of self-assembly was studied to designate H-aggregates (Altoom et al., 2021) as proved by hypsochromic shifting monitored for the fluorescence band upon switching from gel to the corresponding sol phase of **4b** in *n*-butanol as illustrated in Fig. 3. In supramolecular H-aggregation, each molecule interacts with the neighboring molecules via π stacks of aryl groups in cooperation with van der Waals attraction of ether tails to designate the tendency of molecular aggregation to 2D nanofibrous scaffolds (Radwan et al., 2021).

Quantum yields and fluorescence wavelengths of **4b** and **4c** in both gel and sol phases in different solvents are summarized in Table 4. The formed organogels showed different emissions in comparison to the sol phases. In *n*-butanol, the fluorescence intensity of **4b** was monitored at 295 nm in sol, which shifted to 287 nm in gel. However, the incomplete gels showed lower shifting in fluorescence wavelength in comparison the complete gelation. The quantum yields of **4b** and **4c** were generally observed to improve in gel phases higher than sol phases.

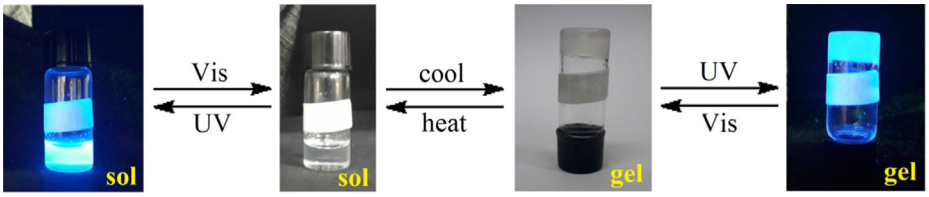

Fig. 2 Thermally reversible fluorescent organogel **4b** in *n*-butanol as described by the "stable to inversion" practice; the solution of **4b** in *n*-butanol (1.86 mM) was heated to ~ 117 °C and then cooled to room temperature; Vis represents visible light and UV represent ultraviolet light; both solution and organogel states were represented by Sol and Gel, respectively.

3.4. Morphological studies

The aggregation morphologies of the dried xerogel from gelator **4b** in *n*-butanol were examined by SEM images to illustrate three dimensional nanofibrous bundles with diameters of 350–550 nm **(**Fig. 4**)**. The assembly process of compound **4b** introduced nanofibrous entanglements. The insertion of ether tails in the skeleton of the organogelator is vital for higher stability of organogelator. Additionally, the fluoro-atoms existing on the rigid aromatic core could also increase the stability of the produced scaffolds (Abdelrahman et al., 2021; Alsoliemy et al., 2021). The generated xerogel showed strong and porous scaffolds due to immobilization of the solvent molecules.

3.5. Thermal stability

The thermal stability was explored by investigating MGC as illustrated in Fig. 5. The melting point of the gel increases in the range of 35–48 °C with increasing the gelator content in the range of 1.86–9.62 mmol/L. The improved thermal stability can be ascribed to the increased density of gelator molecules in the nanofibrous bulk (Khattab et al., 2018). However, the melt point of the gel decreased with increasing the gelator concentration > 9.62 mmol L^{-1}. Increasing the gel-to-sol temperature could be attributed to extending the one-dimensional nanofibrous aggregates leading to better flexibility and higher nanofibrous entanglements, which result in higher transition temperature (Abualnaja et al., 2021).

To examine the thermal reversibility, the solid-like gel was heated to boil point (~117 °C for *n*-butanol) till a transparent solution is monitored. Upon collapsing the gel, the temperature was then reported. The transparent fluid was left to settle down at room temperature to regenerate organogel as verified by the "stable to inversion" approach. The above procedure was repeated to designate no variations in gel → sol temperatures proving good reversibility cycles without fatigue **(**Fig. 6**)**.

3.6. Biological properties

To study the potential utility of the currently synthesized oxadiazole-based gelators for biomedical applications, the cytotoxic properties and antibacterial activity were evaluated (Khattab et al., 2021). The cytotoxic activity (*in vitro*) was studied by monitoring the growing of normal human fibroblast skin cells (BJ1) in the presence of the alkoxy-substituted 2-(biphenylyl)-5-(perflurophenyl)-1, 3, 4-oxadiazole derivatives. No change was detected in cell growth for the oxadiazole derivatives with alkoxy chains with highest length, including **4b** and **4c**. However, the viability started to decrease for the oxadiazole derivative **4a** providing 89.37% viable cells, which was found to further decrease to 85.61 % for the oxadiazole derivative **4a** with the lowest length of alkoxy chain. This relative decrement in the cellular number is not interrelated to cellular death, but may be assigned to the precipitation affinity of oxadiazole derivative leading to reduced spaces for cell growing (Al-Qahtani et al., 2022). Hence, it can be concluded that the

Table 3 Formation of organogels from alkoxy-substituted 2-(biphenylyl)-5-(perflurophenyl)-1, 3, 4-oxadiazole organogelators in different solvents.

Solvent	4a	4b	4c
n-Propanol	P	S	S
n-Butanol	PG	G (1.86)	PG
n-Octanol	PG	G (2.61)	G (2.42)
Ethylacetate	S	S	S
Chloroform	S	S	S
Dichloromethane	S	S	S
Toluene	P	G (3.14)	PG
1,2-Dichloroethane	PG	G (5.07)	G (7.33)
CH_3CN	P	PG	PG
Dimethylsulfoxide	PG	PG	PG
THF	P	PG	PG

S: solution; PG: partial gel; G: gel; P: precipitate. The critical gel concentration (mM) displayed between parentheses.

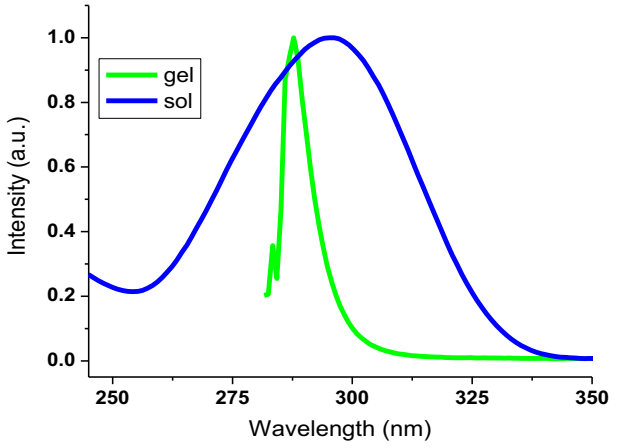

Fig. 3 Normalized emisson of **4b** in the gel and sol (2.44×10^{-5} mol/L) in *n*-butanol.

Table 4 Quantum yield and fluorescence wavelength of **4b** and **4c** in both gel (and partial gel) and sol (2.44×10^{-5} mol/L).

Solvent	4b				4c			
	solution		organogel		solution		organogel	
	λ_{em} (nm)	Φ_F	λ_{em} (nm)	Φ_F	λ_{em} (nm)	Φ_F	λ_{em} (nm)	Φ_F
n-Propanol	297	0.33	290	0.55	306	0.40	294	0.65
n-Butanol	295	0.41	285	0.66	306	0.36	289	0.62
n-Octanol	299	0.40	288	0.78	305	0.24	295	0.52
Acetonitrile	297	0.29	284	0.24	298	0.17	293	0.24
1,2-Dichloroethane	294	0.35	282	0.57	302	0.25	294	0.31
Tetrahydrofuran	295	0.22	285	0.26	300	0.12	292	0.16
Toluene	291	0.30	280	0.45	295	0.22	288	0.46
Dimethylsulfoxide	295	0.49	282	0.53	299	0.41	290	0.50

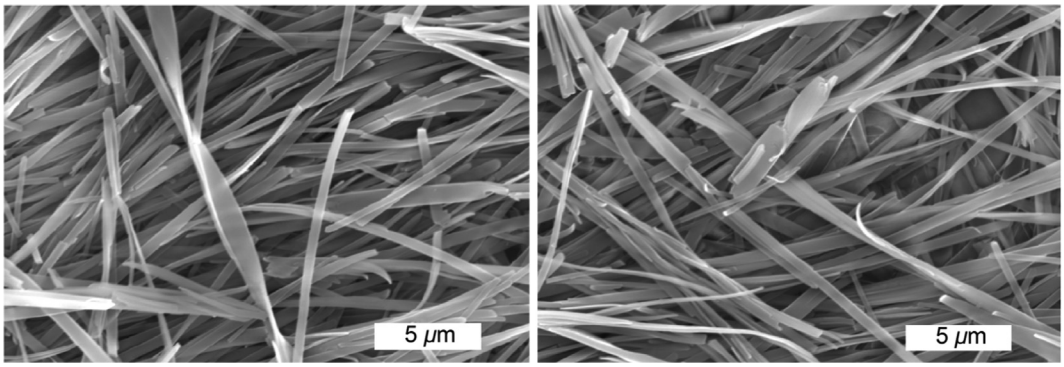

Fig. 4 SEM studies of the xerogel generated from the organogel of **4b** in *n*-butanol (1.86 mM).

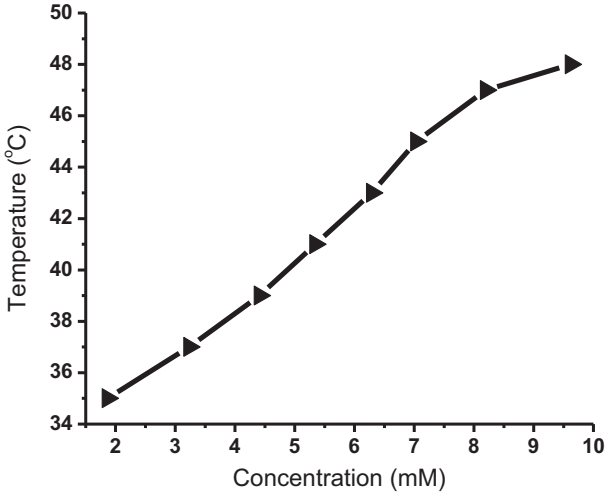

Fig. 5 Gel-to-sol temperatures versus organogelator content for **4b** in *n*-butanol.

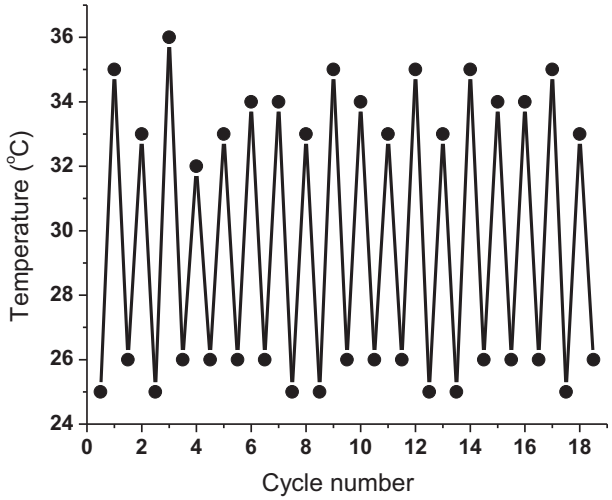

Fig. 6 Temperature-dependent reversibility of **4b** between gel → sol cycles.

current alkoxy-substituted 2-(biphenylyl)-5-(perflurophenyl)-1, 3, 4-oxadiazoles are nontoxic materials. Table 5 displays the antibacterial activity of the oxadiazole gelators **4a-c**. The antibacterial activity of compound **4b** with the best gelation properties was also examined versus ***E. coli*** and ***S. aureus*** using the plate agar count technique to display improved antibacterial activities demonstrating antibacterial reduction (%) of 18 ± 1.3 for ***S. aureus*** and 22 ± 1.5 for ***E. coli***. The antibacterial activity was found to improve with increasing the aliphatic chain length. This can be attributed to the increased solubility of the gelator with increasing the aliphatic chain length. The current oxadiazole organogelators verified to be effective noncytotoxic compounds for potential bioimaging and antibacterial purposes.

Table 5 Antibacterial activity of the oxadiazole gelators.

Sample	Bacterial Reduction %	
	E. coli	*S. aureus*
4a	19 ± 1.0	16 ± 1.4
4b	22 ± 1.5	18 ± 1.3
4c	24 ± 1.3	21 ± 1.1

4. Conclusion

In conclusion, we described the first example of alkoxy-substituted fluorescent LMWO derived from 2-(biphenylyl)-5-(perflurophenyl)-1, 3, 4-oxadiazole as rod-like aromatic segment with the capability to immobilize a diversity of organic solvents. New 1, 3, 4-oxadiazole derivatives with fluorinated aryl moieties bearing different alkoxy chains were synthesized and characterized. Both photophysical and gelation properties were explored. The 2-biphenyl-substituted 1, 3, 4-oxadiazole skeleton was prepared by adding the oxadiazole ring into the biphenyl moiety with the fitting terminal functional group. A suitable synthesis of the perfluorinated phenyl ring bearing ether group was accomplished in high yield via S_NAr chemistry. The chemical structures of the alkoxy-substituted oxadiazole derivatives were proved with $^{1}H/^{13}C/^{19}F$ NMR, elemental analysis and FT-IR spectral analysis. The absorbance and emission spectra showed positive solvatochromic properties. The absorption and emission maxima of the prepared organogelators were detected in the ranges of 260–289 nm and 278–305 nm, respectively. The hexyloxy-substituted 2-(biphenylyl)-5-(perflurophenyl)-1, 3, 4-oxadiazole gelator displayed the best gelation properties in different solvents with critical gel concentrations of 1.86–5.07 mM. Both of π-π stack of rigid aromatic core in cooperation with van der Waals attraction of terminal ether units were able to form stable nanofiber-like supramolecular architectures (350–550 nm) as proved by SEM images and emission spectra of sol–gel phases.

Declaration of Competing Interest

The authors declare that they have no known competing financial interests or personal relationships that could have appeared to influence the work reported in this paper.

Acknowledgements

Princess Nourah bint Abdulrahman University Researchers Supporting Project number (PNURSP2022R22), Princess Nourah bint Abdulrahman University, Riyadh, Saudi Arabia.

Data availability

All relevant data are within the manuscript and available from the corresponding author upon request.

References

Abdelrahman, M.S., Khattab, T.A., Kamel, S., 2021. Hydrazone-Based Supramolecular Organogel for Selective Chromogenic Detection of Organophosphorus Nerve Agent Mimic. ChemistrySelect 6, 2002–2009.

Abualnaja, M.M., Hossan, A., Bayazeed, A., Al-Qahtani, S.D., Al-Ahmed, Z.A., Abdel-Hafez, S.H., El-Metwaly, N.M., 2021. Synthesis and self-assembly of new fluorescent cholesteryloxy-substituted fluorinated terphenyls with gel formation and mesogenic phases. J. Mol. Struct. 1251, 132006.

Al-Qahtani, S.D., Snari, R.M., Al-Ahmed, Z.A., Hossan, A., Munshi, A.M., Alfi, A.A., El-Metwaly, N.M., 2022. Novel halochromic hydrazonal chromophore immobilized into rice-straw based cellulose aerogel for vapochromic detection of ammonia. J. Mol. Liq. 350, 118539.

Alsoliemy, A., Alrefaei, A.F., Almehmadi, S.J., Almehmadi, S.J., Hossan, A., Khalifa, M.E., El-Metwaly, N.M., 2021. Synthesis, characterization and self-assembly of new cholesteryl-substitued sym-tetrazine: Fluorescence, gelation and mesogenic properties. J. Mol. Liq. 342, 117543.

Altoom, N.G., 2021. Synthesis and characterization of novel fluoroterphenyls: self-assembly of low-molecular-weight fluorescent organogel. Luminescence 36, 1285–1299.

Aykent, G., Zeytun, C., Marion, A., Özçubukçu, S., 2019. Simple tyrosine derivatives act as low molecular weight organogelators. Sci. Rep. 9, 1–8.

Bidusenko, I.A., Schmidt, E.Y., Ushakov, I.A., Orel, V.B., Absalyamov, D.Z., Vitkovskaya, N.M., Trofimov, B.A., 2020. Head-to-Tail Dimerization of 4-Fluoroacetophenone in the KOH/DMSO Superbase Suspension and Related SNAr Reaction. Eur. J. Org. Chem. 2020, 3480–3485.

Fan, Q., Méndez-Romero, U.A., Guo, X., Wang, E., Zhang, M., Li, Y., 2019. Fluorinated Photovoltaic Materials for High-Performance Organic Solar Cells. Chem. Asian J. 14, 3085–3095.

Feng, Z., Chen, F., Zhang, X., 2012. Copper catalyzed cross-coupling of iodobenzoates with bromozinc-difluorophosphonate. Org. Lett. 14, 1938–1941.

Fouad, F., Davis, D.R., Twieg, R., 2018. 2-(4-Biphenylyl)-1, 3, 4-oxadiazoles: synthesis and mesogenic studies. Liq. Cryst. 45, 1508–1517.

Ghasemi, Z., Azizi, S., Salehi, R., Kafil, H.S., 2018. Synthesis of azo dyes possessing N-heterocycles and evaluation of their anticancer and antibacterial properties. Monatsh. Chem. 149, 149–157.

Glomb, T., Świątek, P., 2021. Antimicrobial Activity of 1, 3, 4-Oxadiazole Derivatives. Int. J. Mol. Sci. 22, 6979.

Gong, X., Zhang, H., Jiang, N., Wang, L., Wang, G., 2019. Oxadiazole-based 'on-off'fluorescence chemosensor for rapid recognition and detection of Fe2+ and Fe3+ in aqueous solution and in living cells. Microchem. J. 145, 435–443.

Guerre, M., Taplan, C., Nicolaÿ, R., Winne, J.M., Du Prez, F.E., 2018. Fluorinated vitrimer elastomers with a dual temperature response. J. Am. Chem. Soc. 140, 13272–13284.

Hicks, J., Vasko, P., Heilmann, A., Goicoechea, J.M., Aldridge, S., 2020. Arene C− H Activation at Aluminium (I): meta Selectivity Driven by the Electronics of SNAr Chemistry. Angew. Chem. 132, 20556–20560.

Jedlovská, E., Leško, J., 1994. A simple one-pot procedure for the synthesis of 1, 3, 4-oxadiazoles. Synth. Commun. 24, 1879–1885.

Khattab, T.A., 2018. Synthesis and Self-assembly of Novel s-Tetrazine-based Gelator. Helv. Chim. Acta 101, e1800009.

Khattab, T.A., 2020. From chromic switchable hydrazones to smart materials. Mater. Chem. Phys. 254, 123456.

Khattab, T.A., Tolba, E., Gaffer, H., Kamel, S., 2021. Development of electrospun nanofibrous-walled tubes for potential production of photoluminescent endoscopes. Ind. Eng. Chem. Res. 60, 10044–10055.

Kim, D., Lee, S., Park, D., Cho, Y.S., Choi, S., Nam, Y.S., Kim, J.W., 2020. Fabrication of attractive hectorite nanoplatelets by high-pressure homogenization for shear-responsive reversible rheology modification of organogels. J. Ind. Eng. Chem. 90, 274–280.

Lin, Q., Jiang, X.M., Liu, L., Chen, J.F., Zhang, Y.M., Yao, H., Wei, T.B., 2017. A novel supramolecular organogel based on acylhydrazone functionalized pillar [5] arene acts as an I− responsive smart material. Soft Matter 13, 7222–7226.

Ma, Y., Cametti, M., Džolić, Z., Jiang, S., 2018. AIE-active biscyanostilbene-based organogels for quantitative fluorescence sensing of CO 2 based on molecular recognition principles. J. Mater. Chem. C 6, 9232–9237.

Marti, C., Carreira, E.M., 2003. Construction of Spiro [pyrrolidine-3, 3′-oxindoles]− recent applications to the synthesis of oxindole alkaloids. Eur. J. Org. Chem. 2003, 2209–2219.

Patel, K.D., Prajapati, S.M., Panchal, S.N., Patel, H.D., 2014. Review of synthesis of 1, 3, 4-oxadiazole derivatives. Synth. Commun. 44, 1859–1875.

Peveler, W.J., Packman, H., Alexander, S., Chauhan, R.R., Hayes, L. M., Macdonald, T.J., Cockcroft, J.K., Rogers, S., Aarts, D.G., Carmalt, C.J., Parkin, I.P., 2018. A new family of urea-based low molecular-weight organogelators for environmental remediation: the influence of structure. Soft matter 14, 8821–8827.

Plastina, P., Bonofiglio, D., Vizza, D., Fazio, A., Rovito, D., Giordano, C., Barone, I., Catalano, S., Gabriele, B., 2012. Identification of bioactive constituents of Ziziphus jujube fruit extracts exerting antiproliferative and apoptotic effects in human breast cancer cells. J. Ethnopharmacol. 140, 325–332.

Radwan, A.S., Makhlouf, M.M., 2021. Synthesis, characterization, and self-assembly of fluorescent fluorine-containing liquid crystals. Luminescence 36, 1751–1760.

Ragni, R., Punzi, A., Babudri, F., Farinola, G.M., 2018. Organic and organometallic fluorinated materials for electronics and optoelectronics: a survey on recent research. Eur. J. Org. Chem. 2018, 3500–3519.

Salahuddin Mazumder, A., Yar, M.S., Mazumder, R., Chakraborthy, G.S., Ahsan, M.J., Rahman, M.U., 2017. Updates on synthesis and biological activities of 1, 3, 4-oxadiazole: a review. Synth. Commun. 47, 1805–1847.

Sasaki, T., Egami, A., Yajima, T., Uekusa, H., Sato, H., 2018. Unusual Molecular and Supramolecular Structures of Chiral Low Molecular Weight Organogelators with Long Perfluoroalkyl Chains. Cryst. Growth Des. 18, 4200–4205.

Tandon, V.K., Chhor, R.B., 2001. An efficient one pot synthesis of 1, 3, 4-oxadiazoles. Synth. Commun. 31, 1727–1732.

Tominaga, M., Hyodo, T., Maekawa, Y., Kawahata, M., Yamaguchi, K., 2020. One-Step Synthesis of Cyclophanes as Crystalline Sponge and Their [2] Catenanes through SNAr Reactions. Chem. Eur. J. 26, 5157–5161.

Vaidya, A., Pathak, D., Shah, K., 2021. 1, 3, 4-oxadiazole and its derivatives: A review on recent progress in anticancer activities. Chem. Biol. Drug Des. 97, 572–591.

Verma, G., Khan, M.F., Akhtar, W., Alam, M.M., Akhter, M., Shaquiquzzaman, M., 2019. A review exploring therapeutic worth of 1, 3, 4-oxadiazole tailored compounds. Mini Rev. Med. Chem. 19, 477–509.

Yamada, S., Hashishita, S., Asai, T., Ishihara, T., Konno, T., 2017. Design, synthesis and evaluation of new fluorinated liquid crystals bearing a CF 2 CF 2 fragment with negative dielectric anisotropy. Org. Biomol. Chem. 15, 1495–1509.

Zhang, H., Cao, H., Chen, M., Zhang, L., Jiang, T., Chen, H., Li, F., Zhu, S., Yang, H., 2017. Effects of the fluorinated liquid crystal molecules on the electro-optical properties of polymer dispersed liquid crystal films. Liq. Cryst. 44, 2301–2310.

Zhang, X., Zhi, D., Sun, L., Zhao, Y., Tiwari, M.K., Carmalt, C.J., Parkin, I.P., Lu, Y., 2018. Super-durable, non-fluorinated superhydrophobic free-standing items. J. Mater. Chem. A 6, 357–362.

Zhang, Y.P., Wang, B.X., Yang, Y.S., Liang, C., Yang, C., Chai, H. L., 2019. Synthesis and self-assembly of chalcone-based organogels. Colloids Surf. A Physicochem. Eng. 577, 449–455.